Electronic Supplementary Material (ESI) for Nanoscale Advances.
This journal is © The Royal Society of Chemistry 2023

Supporting Information

Regulating the Surface Topography of CpG Nanoadjuvant via Coordination-Driven Self-assembly for Enhanced Tumor Immunotherapy

Li Zhang, Lingpu Zhang, Yuqi Wang, Kai Jiang, Chao Gao, Pengfei Zhang, Yujie Xie, Bin Wang, Haihua Xiao*, and Jie Song*

Materials. CpG-B (5'-TCCATGACGTTCCTGACGTT-3', 20 nt, 6059.0 g mol^{-1}, purification: ULTRAPAGE) and FAM-labeled CpG (FAM-5'-TCCATGACGTTCCTGACGTT-3', 20 nt, 6596.6 g mol^{-1}, purification: HPLC) were purchased from Sangon Biotech (Shanghai) Co., Ltd. Ferrous chloride tetrahydrate ($FeCl_2 \cdot 4H_2O$, purity≥99.0%, 198.81 g mol^{-1}), magnesium chloride hexahydrate ($MgCl_2 \cdot 6H_2O$, purity≥99.0%, 203.3 g mol^{-1}) were purchased from Sigma-Aldrich (Shanghai) Trading Co., Ltd. Hoechst 33258 (Ex/Em: 352/461 nm), LysoTracker Red DND-99 (Ex/Em: 577/590 nm), CellTracker™ Deep Red (Ex/Em: 630/660 nm) were from Invitrogen. Dulbecco's modified eagle medium (DMEM, [+] 4.5 g L^{-1} D-glucose, [+] L-glutamine, [-] sodium pyruvate), fetal bovine serum (FBS), penicillin-streptomycin (P/S, [+] 5000 units mL^{-1} penicillin, [+] 5000 units mL^{-1} streptomycin), and Trypsin-EDTA solution were purchased from Gibco. 3-(4,5-dimethylthiazol-2-yl)-2,5-diphenyltetrazolium bromide (MTT, >98%), calcein AM and ethidium homodimer-1 (EthD-1) live/dead viability kit and phosphate-buffered saline (PBS, pH 7.2-7.4, 0.01 M) were from Solarbio. Ultrapure water was used throughout this research.

Instruments. NanoDrop One microvolume UV-Vis spectrophotometer (Thermo Scientific) was used for the concentration measurement of the DNA solution. G-Storm gradient PCR (Bio-Rad Laboratories, Inc.) was used for the constant temperature heating process. A circular dichroism spectrometer (Applied Photophysics Chirascan V100, Applied Photophysics) was used to characterize the assembly process. Transmission electron microscope (JEM-2100F, JEOL), scanning electron microscope (S-4800, Hitachi), and particle and molecular charge analyzer with a 633 nm He-Ne laser (Zetasizer Nano ZS ZEN3600, Malvern) were used to characterize the morphology, size and zeta potential of the synthesized nanoparticles. Flow cytometry (CytoFLEX LX, Beckman Coulter) with a 488 nm laser was used for the cellular uptake efficiency of FAM-labeled nanoparticles. Toptica confocal laser scanning microscope

with 405, 488, 561, and 640 nm solid laser (CSU-W1-SoRa, Nikon) was used for cell fluorescence imaging. Real-time qPCR analysis (Bio-Rad Laboratories, Inc.) was used for the gene profiling.

Table S1. Feeding ratios of four structural CpG NPs

Samples	C_{CpG} [μM]	$C_{Fe^{2+}}$ [mM]	Molar ratio (CpG: Fe^{2+})	Solvent
NP^{sp}	10	4	1: 400	ddH_2O
NP^{ur}	10	2	1:200	$ddH_2O + Mg^{2+}$
NP^{po}	10	8	1: 800	Tris buffer + Mg^{2+}
NP^{bu}	80	80	1: 1000	Tris buffer + Mg^{2+}

Table S2. Hydrodynamic sizes of CpG NPs determined by DLS

Samples	In ddH_2O		In PBS	
	Effective diameter [nm]	Polydispersity	Effective diameter [nm]	Polydispersity
NP^{sp}	173.7	0.20	158.7	0.21
NP^{ur}	132.1	0.39	121.7	0.47
NP^{po}	168.0	0.55	138.0	0.07
NP^{bu}	216.4	0.26	177.7	0.35

Table S3. Forward and reverse primers used for gene profiling

Gene	Primer	
ATCB	Forward	5'-GGCTGTATTCCCCTCCATCG-3'
	Reverse	5'-CCAGTTGGTAACAATGCCATGT-3'
TNF-α	Forward	5'-TGGAACTGGCAGAAGAG-3'
	Reverse	5'-CCATAGAACTGATGAGAGG-3'
IL-12b	Forward	5'-TGTGGAATGGCGTCTCTGTC-3'
	Reverse	5'-AGTTCAATGGGCAGGGTCTC-3'
Arg-1	Forward	5'-GTGGGAATGGAGGACATGGG-3'
	Reverse	5'-GGATTAGCACCTGGTCCCG-3'
Mrc-1	Forward	5'-GTGGAGTGATGGAACCCCAG-3'
	Reverse	5'-CTGTCCGCCCAGTATCCATC-3'

Table S4. Inhibition percentage of M2 markers after incubation with PBS, free CpG, free $FeCl_2$ and four types of CpG NPs for 20 hours.

Samples	Gene expression after incubation with IL-4 for first 20 h		Gene expression after incubation with samples for second 20 h		Inhibition percentage of M2 markers	
	Arg-1	Mrc-1	Arg-1	Mrc-1	Arg-1	Mrc-1
Free CpG	23.81494	9.1942	0.37094	0.03242	98.4%	99.6%
Free $FeCl_2$			0.22633	0.10899	99.0%	98.8%
NP^{sp}			0.09354	0.03242	99.6%	99.6%
NP^{ur}			1.01596	0.044	95.7%	99.5%
NP^{po}			0.07622	0.02742	99.7%	99.7%
NP^{bu}			0.15313	0.04429	99.4%	99.5%

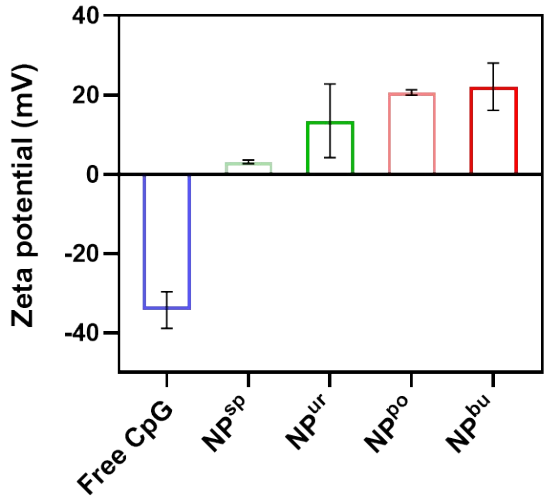

Figure S1. Zeta potentials of free CpG ODNs and CpG NPs.

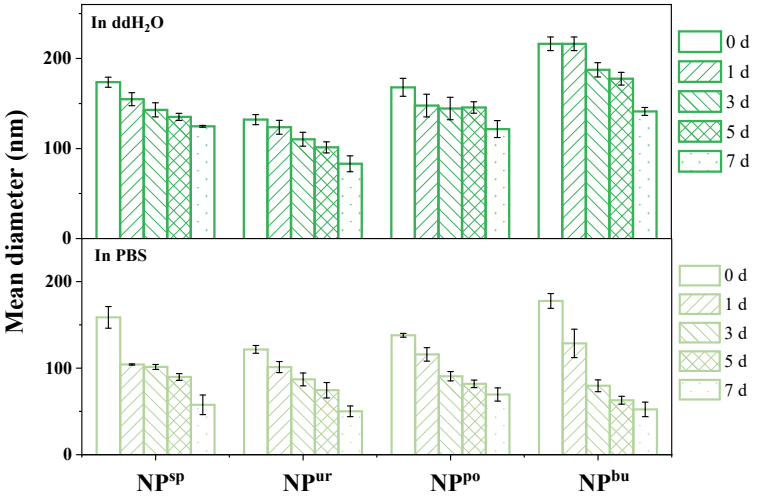

Figure S2. Structural stability of the four CpG NPs in ddH_2O and PBS buffer (pH 7.4) determined by DLS results.

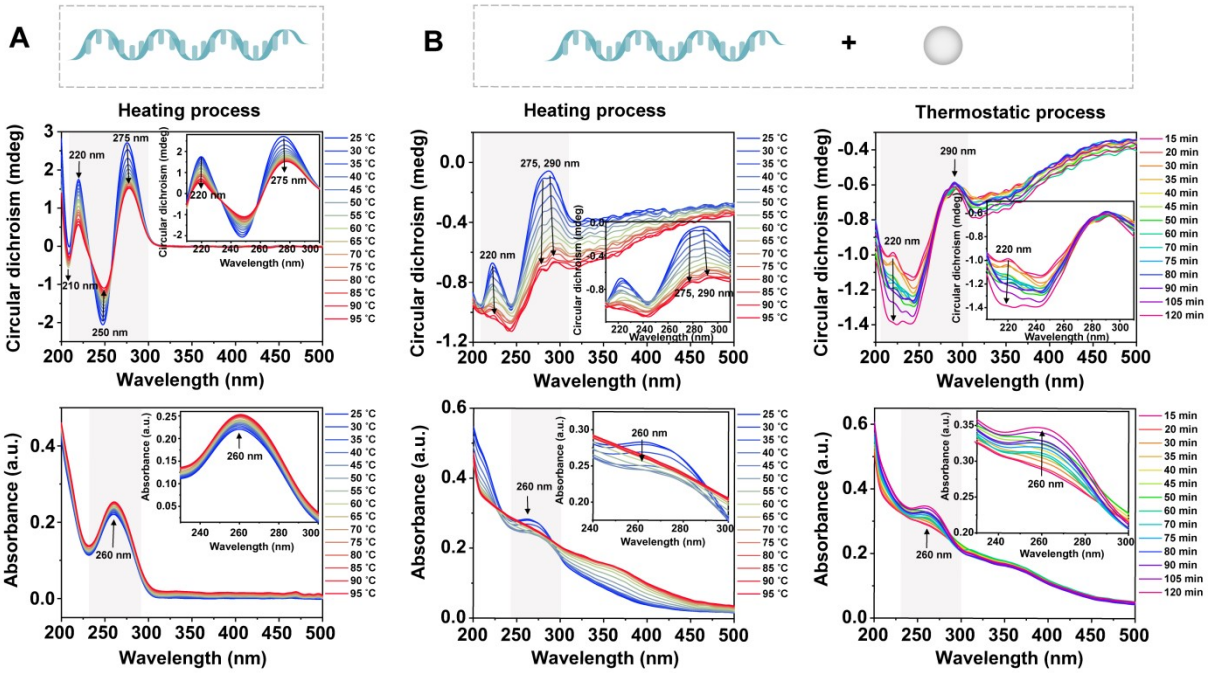

Figure S3. (A) Circular dichroism spectra (top) and ultraviolet-visible spectra (bottom) of free CpG ODNs in a heating process of 25~95 ℃. Insert: amplification of the region corresponding to the characteristic absorption peaks. (B) Circular dichroism spectra (top) and ultraviolet-visible spectra (bottom) of the assembly solution in a heating process of 25~95 ℃ (left) and in a thermostatic process of 95 ℃ (right). Insert: amplification of the region corresponding to the characteristic absorption peaks.

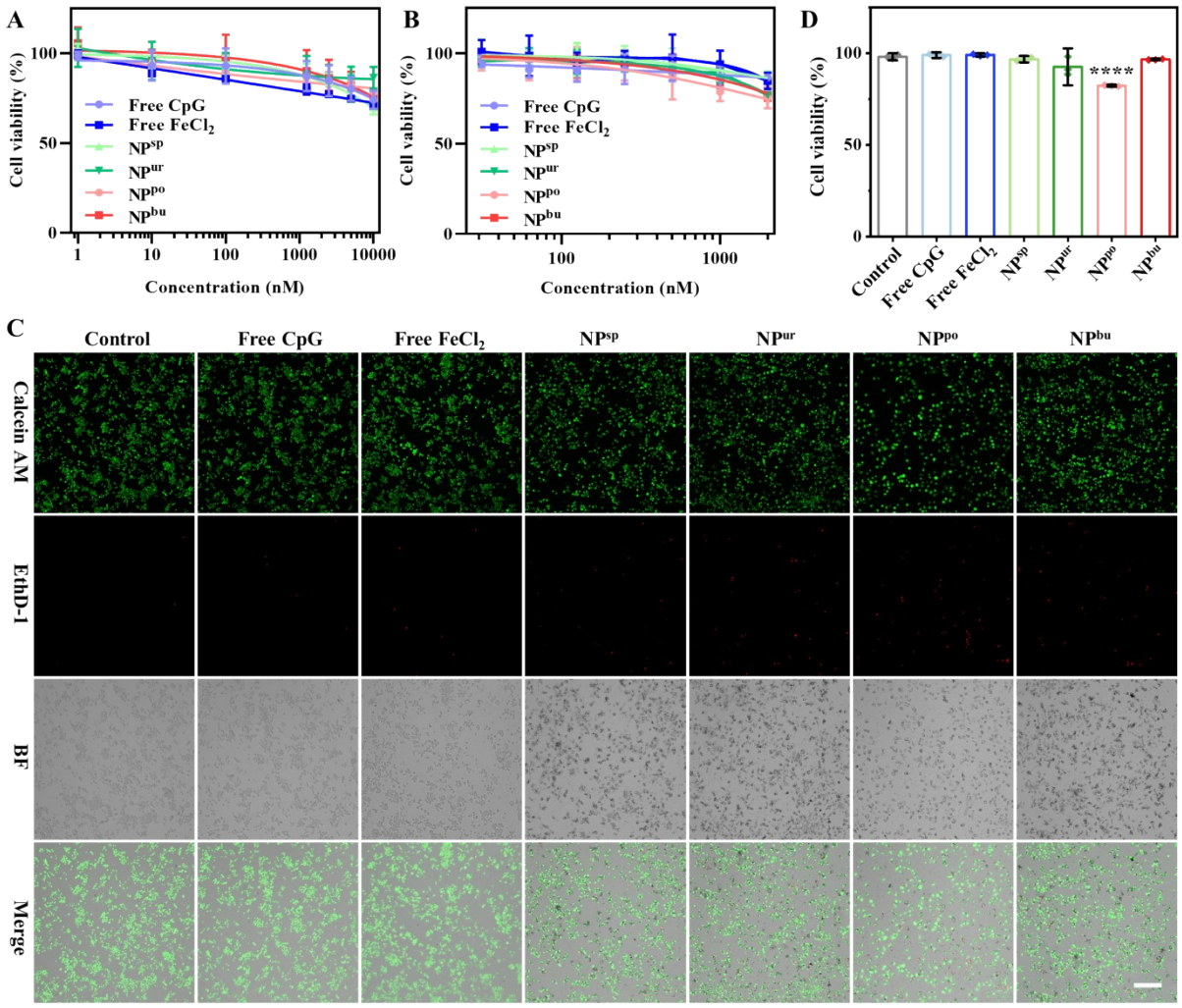

Figure S4. *In vitro* cytotoxicity study of four structural CpG NPs. (A) Macrophage viability after incubation with free CpG, $FeCl_2$, and CpG NPs at a series of CpG concentration gradients (0~10000 nM) for 24 h. (B) Hacat viability after incubation with free CpG, $FeCl_2$, and CpG NPs at a series of CpG concentration gradients (0~2000 nM) for 24 h. Data were shown as mean ± SD (n=6). (C) Fluorescence images of RAW264.7 cells after incubation with free CpG and CpG NPs at CpG equivalent 1000 nM, and 400 μM free $FeCl_2$ for 24 h. The assay stained live cells with calcein-AM (green), and dead cells with ethidium homodimer-1 (red). Scale bars, 200 μm. (D) Macrophage viability calculated from the live/dead cell-stained fluorescent images.

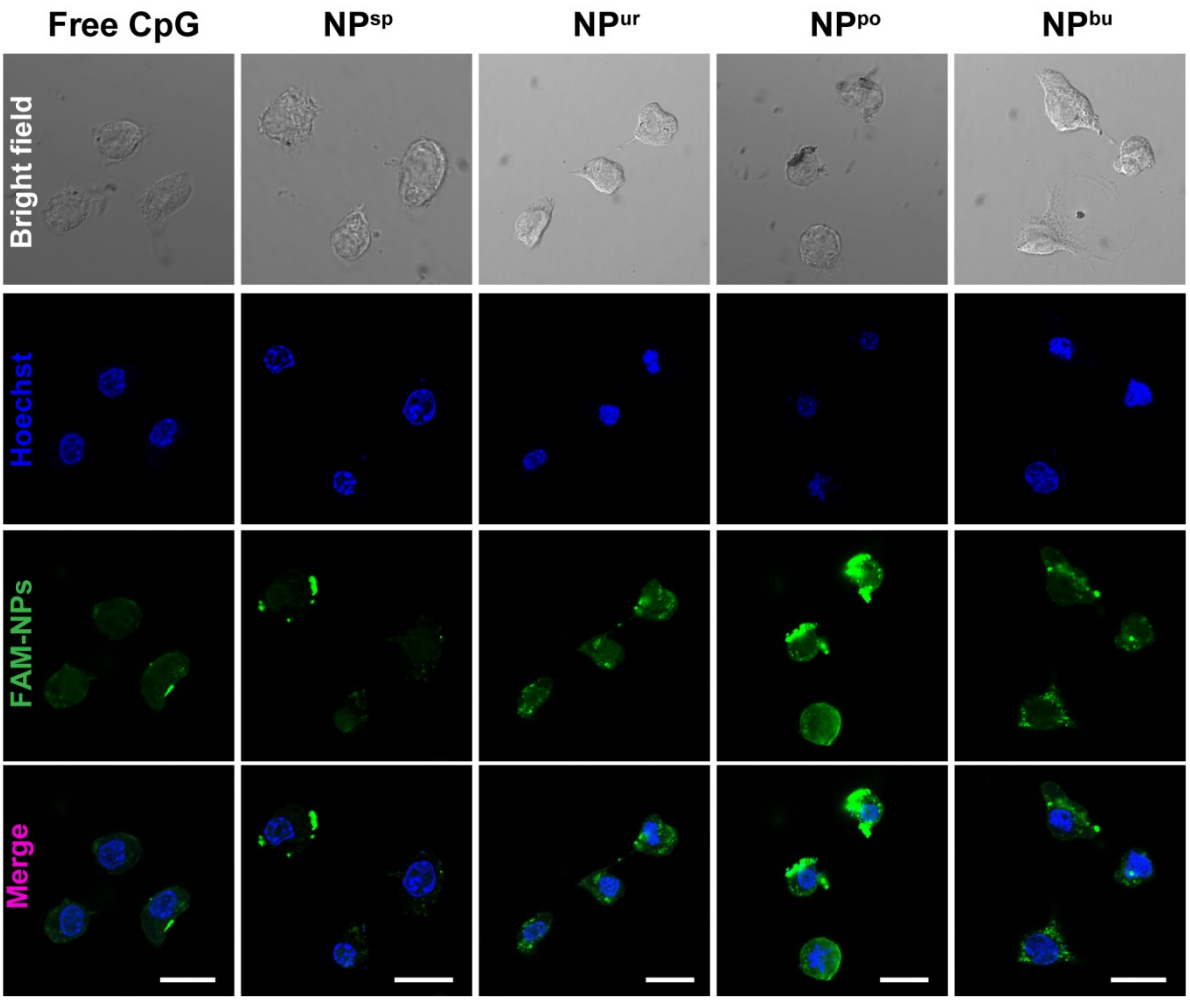

Figure S5. Confocal microscopy images of RAW264.7 cells incubated with free CpG and four CpG NPs for 4 h. Scale bar: 20 μm.

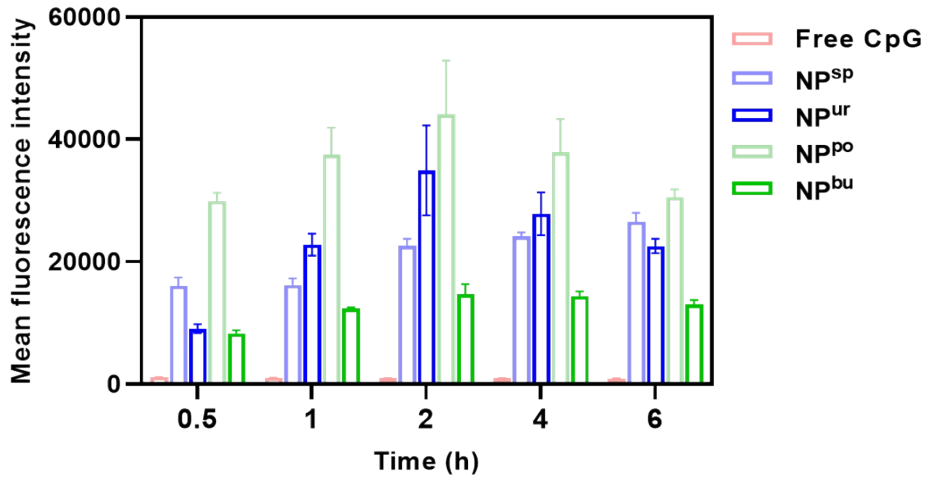

Figure S6. Flow cytometry analysis of the cellular uptake efficiency of free CpG and CpG NPs after different times (0.5, 1, 2, 4, and 6 h) of incubation.

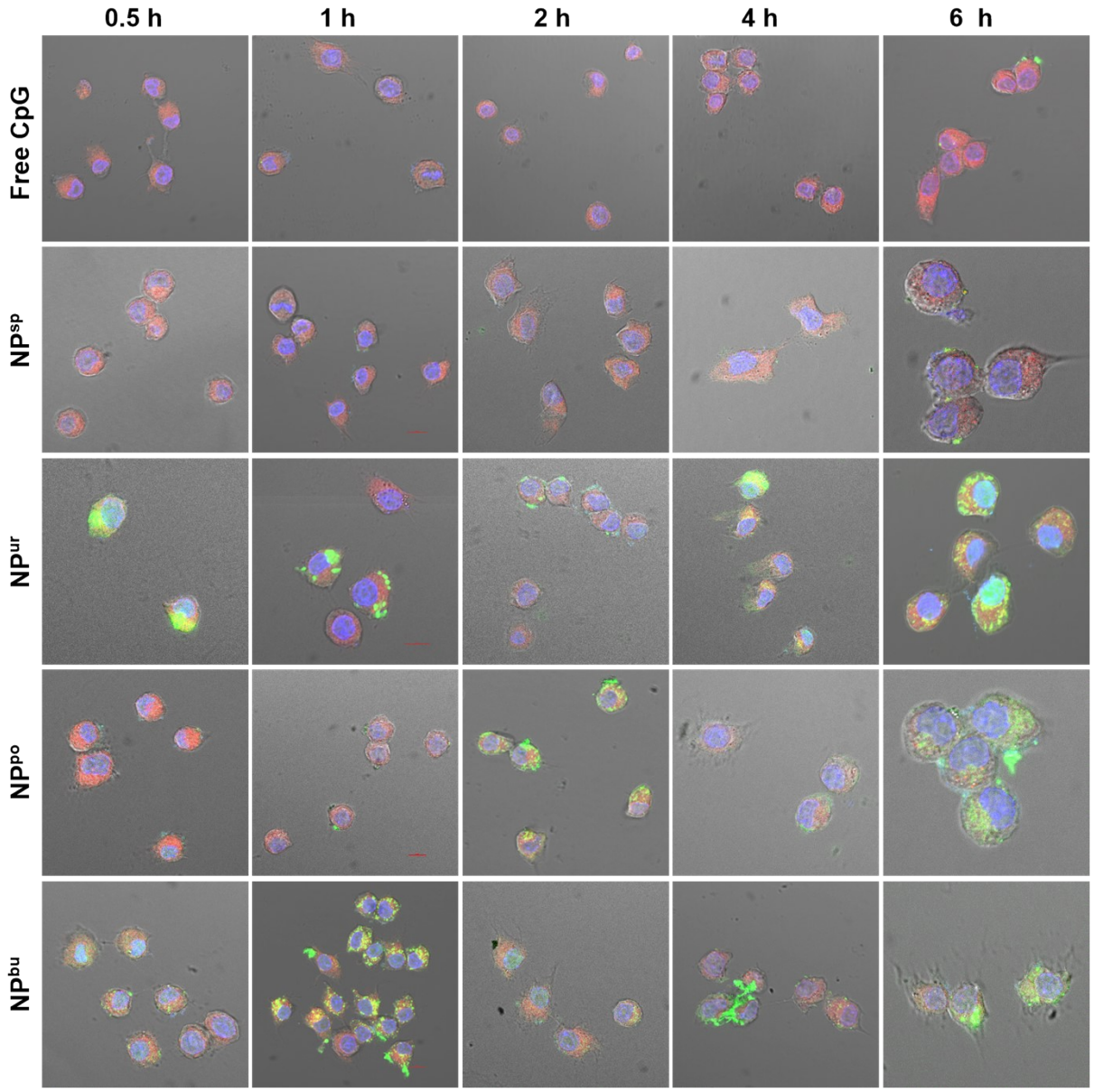

Figure S7. Representative fluorescence images collected from each sample group at each time point for co-location parameter analysis.

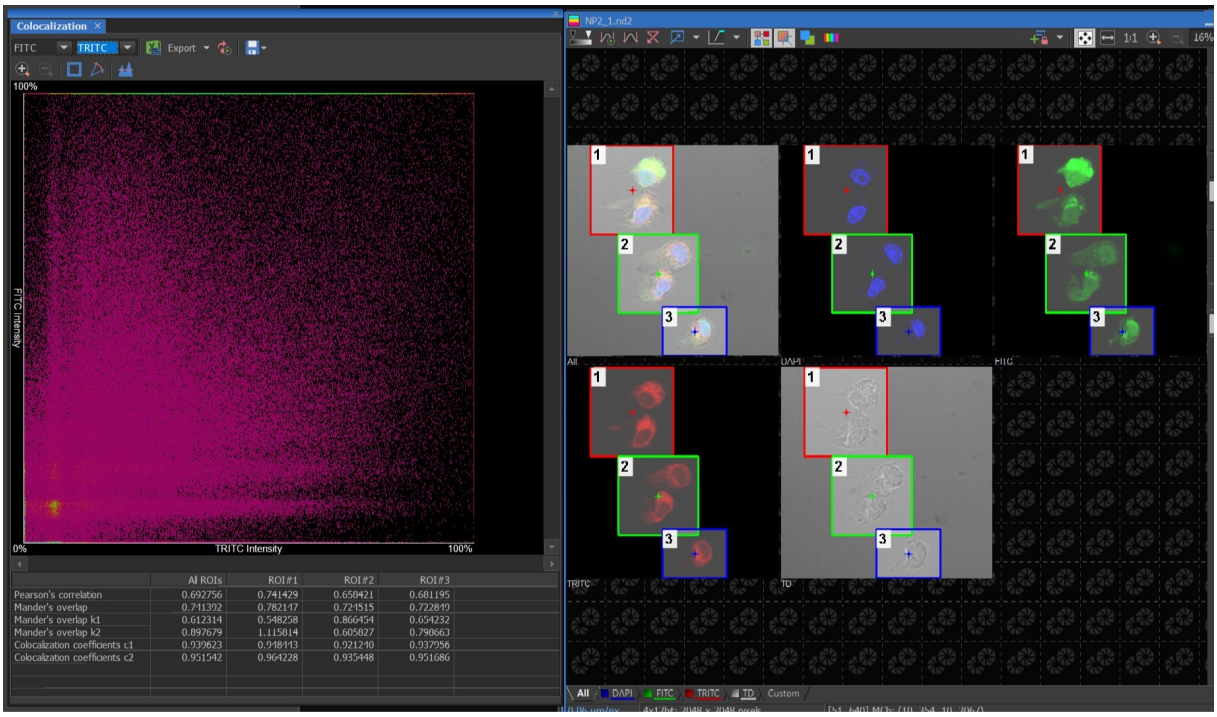

Figure S8. Co-localization parameters (Spearman's correlation and Manders' overlap) between green fluorescent pixels (FAM-labeled CpG) and red fluorescent pixels (LysoTracker) were analyzed by the NIS-Elements Analysis software. The figure above displays the image processing of the representative image captured from the cells treated with NP^{ur} for 4 h.

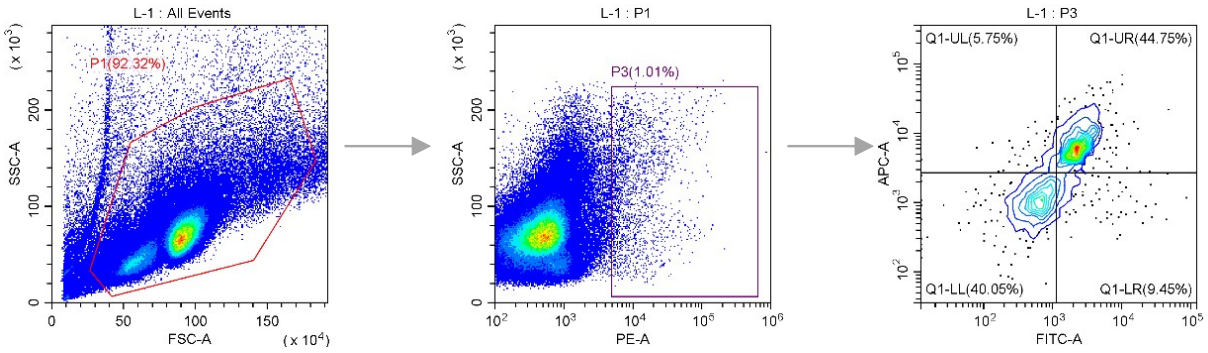

Figure S9. The gating strategy for DC maturation (Figure 4B). B16-OVA mice received intramuscular injections of OVA with different structural CpG NPs. The draining lymph nodes were collected 36 hours later for flow cytometry. Single cells were gated on FSC-A, PE-A and FITC-A.

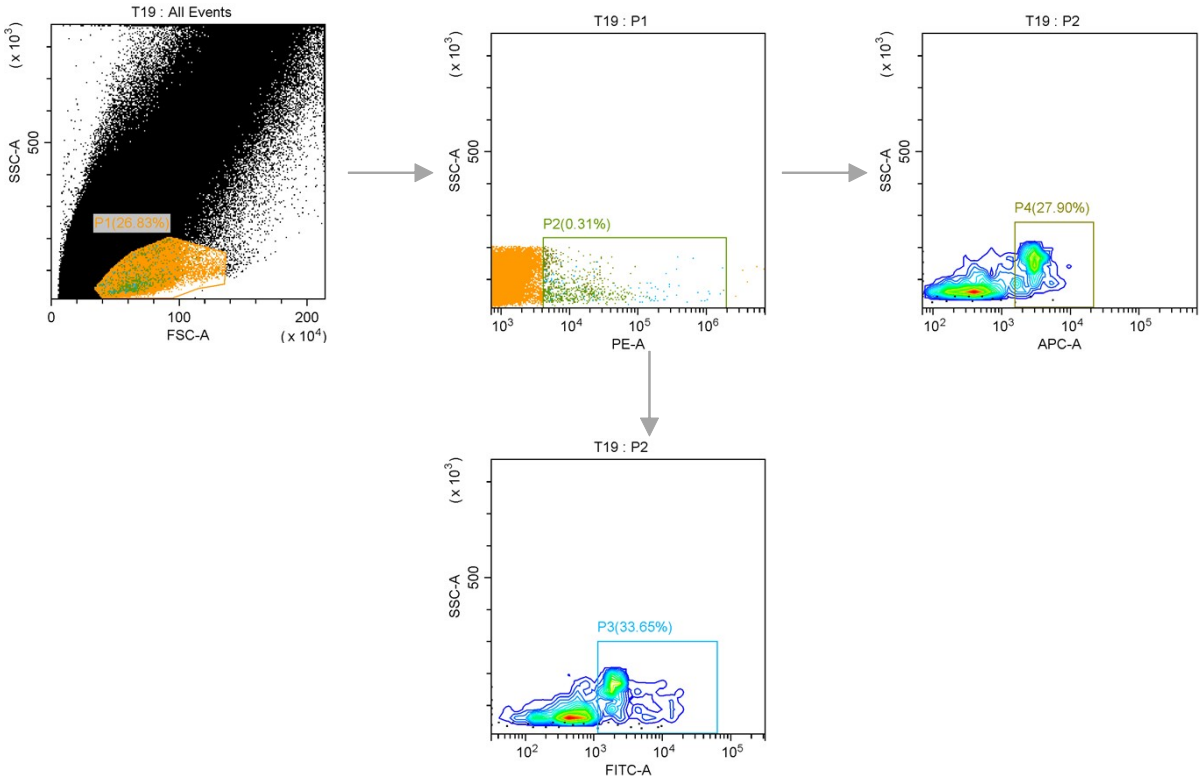

Figure S10. The gating strategy for NK cell response (Figure 4C, D). Single cells were firstly gated in the basis of FSC-A and PE-A, then gated on APC-A and FITC-A.

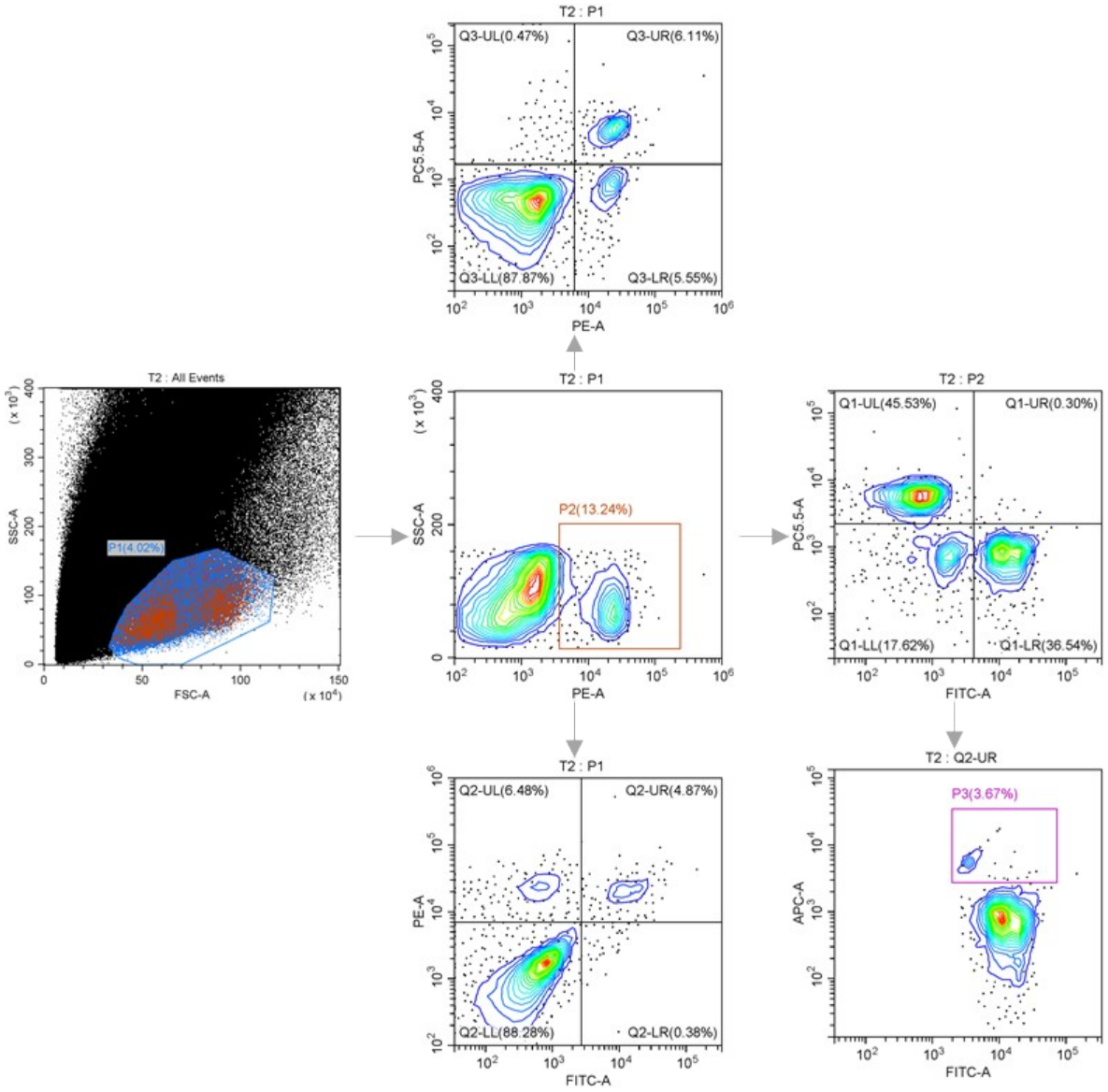

Figure S11. Gating strategies for T cell responses (Figure 4E). Single cells were firstly gated in the basis of FSC-A, then gated on PE-A, follow with FITC-A.

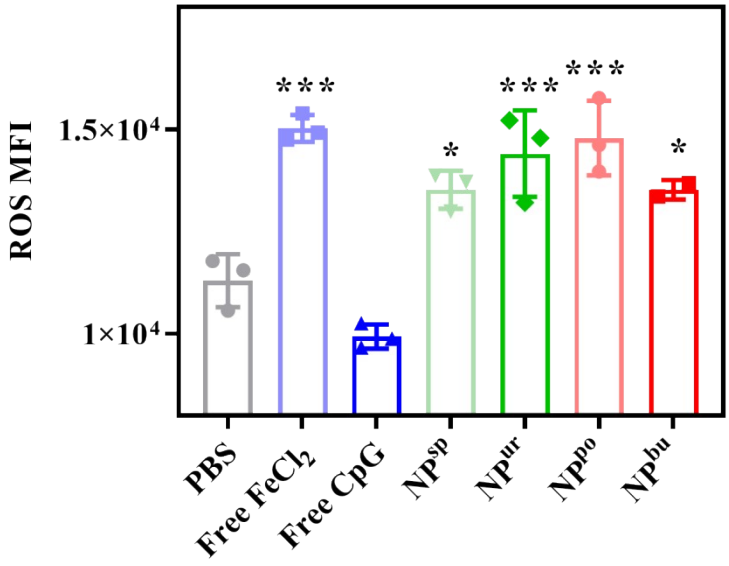

Figure S12. ROS levels in Hacat after incubation with free CpG and CpG NPs at CpG equivalent 1000 nM, and 400 μM free $FeCl_2$ for 24 h.

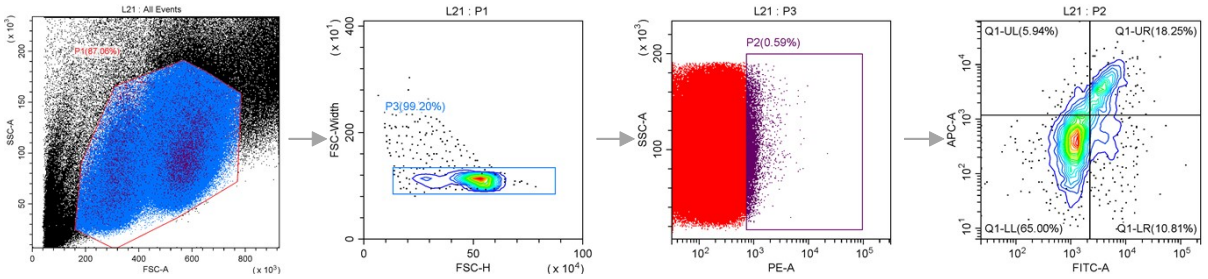

Figure S13. The gating strategy for DC mature (Figure 5F). Single cells were gated on FSC-A, FSC-H, PE-A and FITC-A.

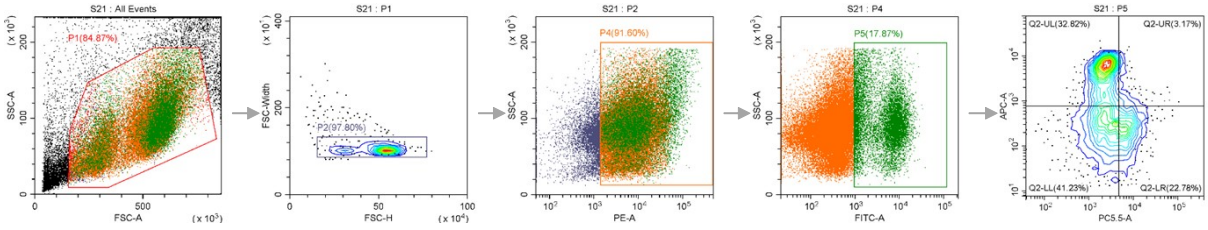

Figure S14. Gating strategies for T cell responses (Figure 5F). Single cells were firstly gated in the basis of FSC-A, FSC-H, PE-A, FITC-A and PC5.5-A.

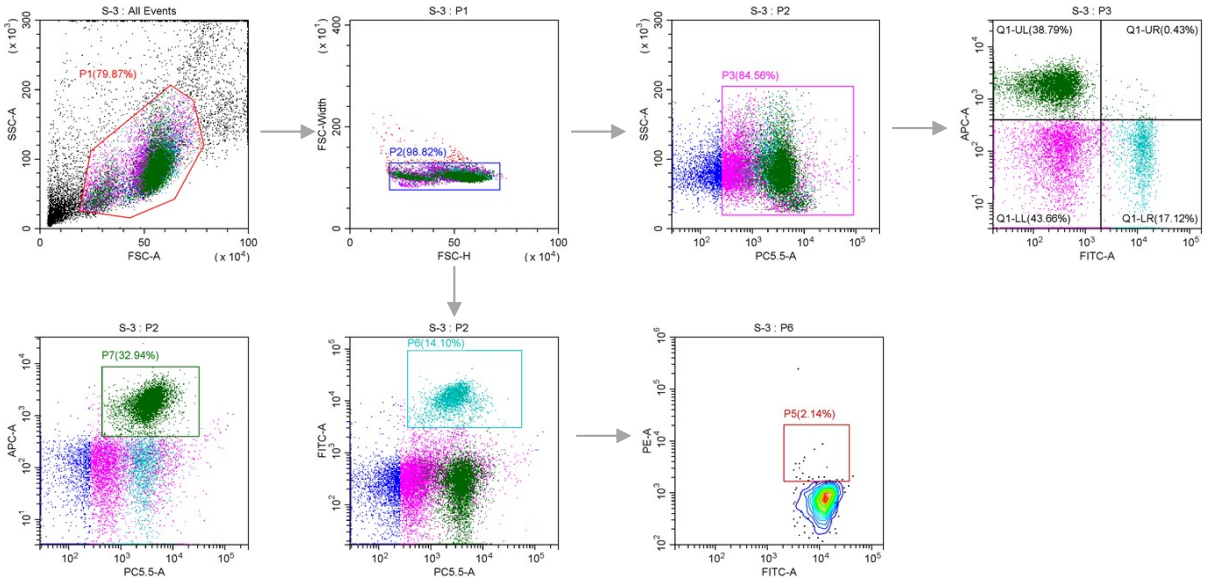

Figure S15. Single cells were gated on FSC-A, FSC-H, PE-A, FITC-A and PC5.5-A for the analysis of expressions of CD4, CD8, and IFN-γ (Figure 5F).